Stress Development in Drying Fibers and Spheres

Herong Lei, Lorraine F. Francis, William W. Gerberich, L. E. Scriven

Department of Chemical Engineering and Materials Science, University of Minnesota, Minneapolis, Minnesota 55455

Received 15 May 2001; accepted 7 April 2003

ABSTRACT: Stress development during drying is a critical factor that affects the final structure and properties of a coated fiber or spherical product. Stress development during drying of the coating is due to nonuniform shrinkage and physical constraints. In this study, a large deformation elasto-viscoplastic model is developed to predict stress development in drying fibers and spheres after the coatings solidify. From the model, stress evolution in the drying fibers/spheres can be predicted by a partial differential equation of diffusion in one dimension, a first-order partial differential equation of pressure distribution, and two ordinary differential equations on local evolution of the stress-free state. The system of equations is solved by the Galerkin/finite element method in the one dimensional axial/spherical symmetric coatings. Solutions show changes in solvent concentration and viscous stress as the coating dries.

Key words: coatings; fibers; stress; yielding

INTRODUCTION

Drying of coated fiber and spherical products has a wide variety of applications. Fine ceramic fibers are used in composites and high temperature resistant textiles for insulation and gas filtering. These ceramic fibers are usually made by spinning a solution that has achieved the required viscosity. Glass optical fibers are widely used to transmit optical signals over long distances. Once these glass fibers are drawn from the hot melt, contact of the fresh fiber with any solid surface results in the immediate formation of microflaws that reduce fiber strength; thus polymer coatings must be applied as thin liquids that solidify by cooling or curing. These protective polymer coatings preserve the inherent strength of the glass and provide the fiber with low micro-bending susceptibility. Similarly, drying of droplets (spheres) is a common practice in dairy and painting industries.

In the above processes, the structure and properties of the final product depend critically on the course of drying, cooling, or curing. Inhomogeneous properties can develop within the fiber/sphere. Defects that exist in the final product are often attributed to polymerization and crosslinking, phase transformation, and stress evolution during coating. Stress development within the fiber/sphere also limits the thickness of the coating that can be applied. Once the coating has solidified, the evaporation of solvent, further reaction, further cooling, and so on may cause considerable volume shrinkage. When the coating is constrained or the shrinkage of the coating is not uniform, internal strain develops, and this strain is accompanied by stress.

Diffusion and mass transfer during drying of fibers and spheres have been widely studied. Drying of fibers and spheres has been examined by Charlesworth et al.,[1] Crank,[2] Okazaki,[3] Sano and Keey,[4] Sano,[5] and Cairncross.[6] Among them, Okazaki[3] and Sano et al.[4,5] employed a mass basis in formulating diffusion and convective mass transfer; Cairncross et al.[6] employed a volume basis.

In this article, the Cairncross[6] volume basis approach to drying fibers and spheres is extended to explore the stress development mechanism after the coating solidifies. An elasto-viscoplastic model is developed to predict stress development from frustrated shrinkage and stress relaxation from the viscoplastic change of the stress-free state. This model is developed for the drying of a cylindrical or spherical body without any substrate (core). It can be readily extended to consider the drying of an annular or spherical shell surrounding a substrate (core), such as the drying of the polymer coating on an optical fiber.

THEORY

Drying and diffusion

For a binary solution consisting of a volatile solvent and a nonvolatile polymer, the original polymer location is identified by its coordinates $\mathbf{X}(R, \Theta, Z)$, with Z specifying the axial coordinate in fibers and the azimuthal angle in spheres (Fig. 1). After drying and deformation, the same polymer is located by its new

Correspondence to: H. Lei, Eastman Kodak Company, Kodak Park, Rochester, NY 14652 (herong.lei@kodak.com).

Journal of Applied Polymer Science, Vol. 90, 3934–3944 (2003)

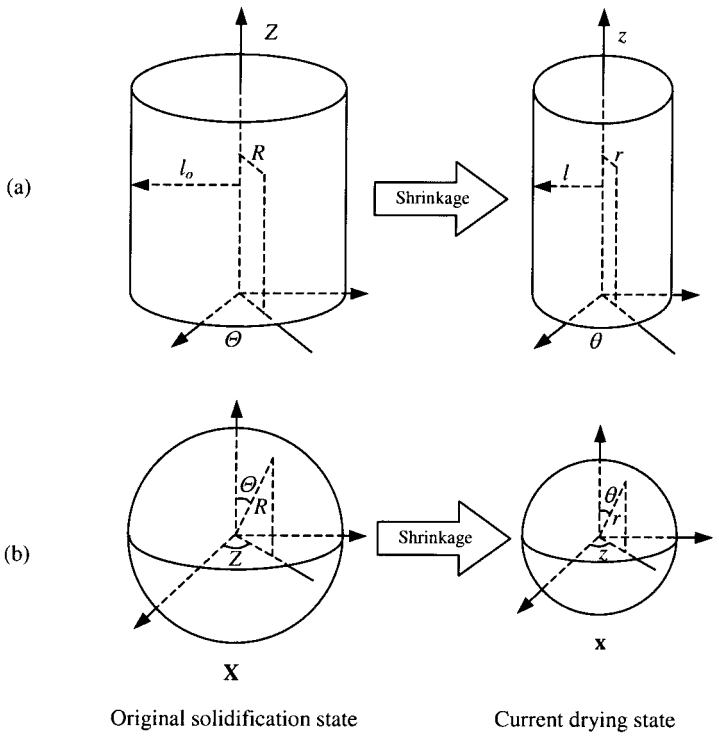

Figure 1 Cylindrical/spherical coordinates in the drying fibers and spheres. The drying and deformation are under axially/centrally symmetric conditions. The fiber is under plane–strain condition.

position $\mathbf{x}(r, \theta, z)$. In the case of uniform initial polymer concentration and uniform drying rate across the coating/air interface, the coating retains its cylindrical/spherical shape, and all coating particles move radially towards the axis/center. This makes the drying cylindrically/centrally symmetric and one dimensional. In the case of ideal mixing, Amagat's law holds and the molar concentration of solvent (c_s) is governed by

$$\frac{\partial c_s}{\partial t} = \frac{1}{r^\omega}\frac{\partial}{\partial r}\left(r^\omega D\,\frac{\partial c_s}{\partial r}\right) \tag{1}$$

in which D is the binary diffusion coefficient and r is the radius in the current spatial coordinate. Following Cairncross[6] notation, the exponent ω is equal to 1 for axially symmetric fibers, and 2 for centrally symmetric spheres.

The boundary conditions to eq. (1) are the following. At the center of the fiber/sphere, the solvent flux is zero. At the free surface, the solvent flux relative to the moving surface on the coating side is equal to that on the air side. The latter is described by a mass transfer coefficient multiplied by a concentration-difference driving force. Therefore

$$D\,\frac{\partial c_s}{\partial r} = 0 \quad \text{at} \quad r = 0, \quad t > 0 \tag{2}$$

$$\frac{D}{1 - c_s\overline{V}_s}\,\frac{\partial c_s}{\partial r} = -k_g(Hc_s - c_g^\infty) \quad \text{at} \quad r = l(t), \quad t > 0 \tag{3}$$

where $\overline{V}_s$ is the partial molar volume of solvent, c_g^∞ is the solvent concentration in the air far from the surface, $c_s(l)$ is the solvent concentration in the coating at the surface and in equilibrium with that in the air at the surface, and H is a solubility coefficient (Henry's coefficient) that depends on temperature. In addition, since the free surface is permeable to the solvent but not to the polymer, and the fiber/sphere is decreasing in size, the polymer on the surface is swept inward. The rate of change of the radius of this interface $l(t)$ is given by

$$\frac{dl(t)}{dt} = -\overline{V}_s k_g(Hc_s - c_g^\infty). \tag{4}$$

Kinematics

Fibers are usually long, with deformation in the axial direction constrained, and therefore deformation is subject to the plane–strain condition. In drying spheres, however, the deformation is centrally symmetric. As in Figure 1, the solidification point, which is stress free, is chosen as the original reference state. When the deformation is cylindrically/centrally symmetric, the total deformation gradient is

$$\mathbf{F} = \nabla_{\mathbf{X}}\mathbf{x} = \mathbf{e}_R\mathbf{e}_r \frac{\partial r}{\partial R} + \mathbf{e}_\Theta\mathbf{e}_\theta \frac{r}{R} + \mathbf{e}_Z\mathbf{e}_z\left(\frac{r}{R}\right)^{\omega-1}, \quad (5)$$

where ($\mathbf{e}_R$, $\mathbf{e}_\Theta$, $\mathbf{e}_Z$) and ($\mathbf{e}_r$, $\mathbf{e}_\theta$, $\mathbf{e}_z$) are respectively unit base vectors in the original reference coordinate $\mathbf{X}(R, \Theta, Z)$ and the current spatial coordinate $\mathbf{x}(r, \theta, z)$. Due to the symmetric condition,

$$\mathbf{e}_r = \mathbf{e}_R, \quad \mathbf{e}_\theta = \mathbf{e}_\Theta, \quad \mathbf{e}_z = \mathbf{e}_Z. \quad (6)$$

Assuming the mechanical deformations (elastic and viscoplastic if yielded) are incompressible, and the volume change is solely due to drying and shrinkage,

$$\det \mathbf{F} = \left(\frac{r}{R}\right)^{\omega}\frac{\partial r}{\partial R} = \alpha^3, \quad (7)$$

where α is the shrinkage factor that is related to the current solvent concentration (c_s) and the solvent concentration at solidification (c_s^*). When drying starts from the solidification point, the initial solvent concentration, $c_s^* = c_s^0$, and

$$\alpha \equiv \left(\frac{1 - c_s^0\bar{V}_s}{1 - c_s\bar{V}_s}\right)^{1/3}. \quad (8)$$

Eq. (7) gives the current position (r) of the coating particle that was originally located at radius R. The boundary condition for r is obvious since the center is not moving; therefore $r = 0$ at $R = 0$.

In eq. (5), the total deformation gradient can be factored into the isotropic volume shrinkage ($\alpha\mathbf{I}$), the elastic deformation gradient ($\mathbf{F}^e$), and the viscoplastic deformation gradient ($\mathbf{F}^{vp}$). After rearrangement, the elastic deformation tensor becomes

$$\mathbf{F}^e = \frac{1}{\alpha}\mathbf{F}\cdot\mathbf{F}^{vp^{-1}} = \frac{\alpha^2}{F_R^{vp}}\left(\frac{R}{r}\right)^{\omega}\mathbf{e}_R\mathbf{e}_R + \frac{1}{\alpha F_\Theta^{vp}}\frac{r}{R}\mathbf{e}_\Theta\mathbf{e}_\Theta + \frac{1}{\alpha F_Z^{vp}}\left(\frac{r}{R}\right)^{\omega-1}\mathbf{e}_Z\mathbf{e}_Z, \quad (9)$$

in which F_R^{vp}, F_Θ^{vp}, F_Z^{vp} are the only nonzero components of the viscoplastic deformation gradient ($\mathbf{F}^{vp}$). The elastic strain can be expressed as either the left or right Cauchy-Green tensors; under axisymmetric/spherical symmetric conditions, the two are the same:

$$\mathbf{C}^e = \mathbf{B}^e = \mathbf{F}^e\cdot\mathbf{F}^{e^T} = B_R^e\mathbf{e}_R\mathbf{e}_R + B_\Theta^e\mathbf{e}_\Theta\mathbf{e}_\Theta + B_Z^e\mathbf{e}_Z\mathbf{e}_Z \quad (10)$$

in which

$$B_R^e = \frac{\alpha^4}{(F_R^{vp})^2}\left(\frac{R}{r}\right)^{2\omega}, \quad B_\Theta^e = \frac{1}{(\alpha F_\Theta^{vp})^2}\left(\frac{r}{R}\right)^2,$$

$$B_Z^e = \frac{1}{(\alpha F_Z^{vp})^2}\left(\frac{r}{R}\right)^{2(\omega-1)} \quad (11)$$

Any difference between the current stress-free state and the current state causes the strain tensor to deviate from the unity tensor; such deviation gives rise to stress.

The viscoplastic strain rate is the time derivative of the viscoplastic deformation gradient in the current stress-free state, with three nonzero components:

$$\bar{D}_R^{vp} = \frac{\dot{F}_R^{vp}}{F_R^{vp}}B_R^e, \quad \bar{D}_\Theta^{vp} = \frac{\dot{F}_\Theta^{vp}}{F_\Theta^{vp}}B_\Theta^e, \quad \bar{D}_Z^{vp} = \frac{\dot{F}_Z^{vp}}{F_Z^{vp}}B_Z^e \quad (12)$$

Eq. (12) describes the viscoplastic relaxation rate of the current stress-free state, which is usually related to the post-yield viscosity and the excess stress level above the yield stress.

Pressure distribution and constitutive relations

Similar to the drying planar coating described by Lei and coworkers,[7] the elastic stress is modeled with the neo-Hookean equation, which for the drying of cylindrically/centrally symmetric forms gives the non-zero components of Cauchy stress as

$$\sigma_r = -\pi + GB_R^e, \quad \sigma_\theta = -\pi + GB_\Theta^e, \quad \sigma_z = -\pi + GB_Z^e \quad (13)$$

Here G is the coating shear modulus, and the components of the Cauchy-Green strain tensor (B_R^e, B_Θ^e, B_Z^e) are given in eq. (11). The lower case subscripts (r, θ, z) in eq. (13) identify three components of the Cauchy stress tensor in the current state. The hydrostatic pressure-like parameter (π) is related to the negative mean normal stress (p) simply by

$$\pi = p + \frac{G}{3}(B_R^e + B_\Theta^e + B_Z^e). \quad (14)$$

When inertia and gravity are negligible, the mechanical equilibrium requires that

$$r\frac{\partial\sigma_r}{\partial r} + \omega(\sigma_r - \sigma_\theta) = 0. \quad (15)$$

In drying axisymmetric fibers ($\omega = 1$) the stress along the axis direction, σ_z, provides the plane-strain constraint. For central symmetric spheres ($\omega = 2$), obviously σ_z equals σ_θ. The substitution of σ_r and σ_θ from eq. (13) into eq. (15) gives the partial differential equation that governs the pressure-like parameter π:

$$\frac{\partial \pi}{\partial r} = G\left[\frac{4}{\alpha}\frac{\partial \alpha}{\partial r}B_R^e + \frac{2\omega\alpha}{r(F_R^{vp})^2}\left(\frac{R}{r}\right)^{\omega-1} - \frac{\omega(B_R^e + B_\Theta^e)}{r} - \frac{2B_R^e}{F_R^{vp}}\frac{\partial F_R^{vp}}{\partial r}\right] \quad (16)$$

To solve eq. (16) for π, a boundary condition is necessary. At the interface between coating and drying air ($r = l(t)$), the normal stress to the surface in the air side and the coating side should be in equilibrium. In this case the surface tension is negligibly small compared to the non-zero components of the stress. This provides the boundary condition on π:

$$\pi = p_a + GB_R^e, \quad \text{at} \quad r = l(t) \quad (17)$$

where p_a is the pressure in the drying air. Since p_a serves only as a basis pressure, it is set to zero in the following derivations.

As the drying continues and stress rises, the coating may enter an elasto-viscoplastic regime. To describe the viscoplastic flow after the coating yields, the Cauchy stress is transformed from the current state to the current stress-free state. Doing so gives the Second Piola-Kirchhoff stress tensor, whose non-zero components are

$$\bar{S}_R = -\frac{\pi\alpha^3}{B_R^e} + G\alpha^3, \quad \bar{S}_\Theta = -\frac{\pi\alpha^3}{B_\Theta^e} + G\alpha^3,$$

$$\bar{S}_Z = -\frac{\pi\alpha^3}{B_Z^e} + G\alpha^3 \quad (18)$$

Yielding is predicted with von Mises' criterion, which is formulated in terms of the second invariant of the current elastic stress. For von Mises' criterion, only the deviatoric part of Cauchy stress needs to be transformed to the current stress-free state:

$$\bar{S}'_R = \frac{G\alpha^3}{3}\left(2 - \frac{B_\Theta^e}{B_R^e} - \frac{B_Z^e}{B_R^e}\right), \quad \bar{S}'_\Theta = \frac{G\alpha^3}{3}\left(2 - \frac{B_R^e}{B_\Theta^e} - \frac{B_Z^e}{B_\Theta^e}\right)$$

$$\bar{S}'_Z = \frac{G\alpha^3}{3}\left(2 - \frac{B_R^e}{B_Z^e} - \frac{B_\Theta^e}{B_Z^e}\right) \quad (19)$$

in which all components are independent of pressure. The second invariant of the above hypothetical stress-state depends on its deviatoric part alone,

$$\Phi = \sqrt{\frac{1}{2}\left[(\bar{S}'_R C_R^e)^2 + (\bar{S}'_\Theta C_\Theta^e)^2 + (\bar{S}'_Z C_Z^e)^2\right]}$$

$$= \frac{G\alpha^3}{3\sqrt{2}}\sqrt{(2B_R^e - B_\Theta^e - B_Z^e)^2 + (-B_R^e + 2B_\Theta^e - B_Z^e)^2 + (-B_R^e - B_\Theta^e + 2B_Z^e)^2} \quad (20)$$

Von Mises' yield criterion is

$$\Phi - k\begin{cases} < 0, & \text{not yielding} \\ = 0, & \text{critical condition} \\ > 0, & \text{continuous yielding} \end{cases}$$

where k is the critical shear stress at yielding and acts to define the size of the (abstract) yield surface in the space of principal stresses (the stress having been transformed to the current stress-free state). When the criterion is exceeded, the flow law of yielding is that the rate of viscoplastic deformation is proportional to the excess of the second invariant over the yield value, and is in the direction, in the space of the principal directions, of the gradient of the second invariant:

$$\bar{D}_R^{vp} = \frac{1}{\mu}\langle\Phi - k\rangle\frac{\partial\Phi}{\partial\bar{S}_R} = \frac{\langle\Phi - k\rangle}{2\mu\Phi}C_R^{e^2}\bar{S}'_R \quad (21)$$

$$\bar{D}_\Theta^{vp} = \frac{1}{\mu}\langle\Phi - k\rangle\frac{\partial\Phi}{\partial\bar{S}_\Theta} = \frac{\langle\Phi - k\rangle}{2\mu\Phi}C_\Theta^{e^2}\bar{S}'_\Theta \quad (22)$$

$$\bar{D}_Z^{vp} = \frac{1}{\mu}\langle\Phi - k\rangle\frac{\partial\Phi}{\partial\bar{S}_Z} = \frac{\langle\Phi - k\rangle}{2\mu\Phi}C_Z^{e^2}\bar{S}'_Z \quad (23)$$

where μ is the post-yield viscosity of the stress-free state. The notation $\langle\ \rangle$ denotes

$$\langle\Phi - k\rangle = \begin{cases} \Phi - k & \text{if } \Phi > k \\ 0 & \text{otherwise} \end{cases}$$

With rearrangement that makes use of eqs. (11, 12, 19–23), these strain rate equations simplify to three ordinary differential equations that govern the development of the current stress-free state:

$$\frac{\dot{F}_R^{vp}}{F_R^{vp}} = \frac{G\alpha^3}{6}\frac{\langle\Phi - k\rangle}{\mu\Phi}(2B_R^e - B_\Theta^e - B_Z^e) \quad (24)$$

$$\frac{\dot{F}_\Theta^{vp}}{F_\Theta^{vp}} = \frac{G\alpha^3}{6}\frac{\langle\Phi - k\rangle}{\mu\Phi}(2B_\Theta^e - B_R^e - B_Z^e) \quad (25)$$

$$\frac{\dot{F}_Z^{vp}}{F_Z^{vp}} = \frac{G\alpha^3}{6}\frac{\langle\Phi - k\rangle}{\mu\Phi}(2B_Z^e - B_\Theta^e - B_R^e) \quad (26)$$

These three equations are not independent. Adding them together gives:

$$\frac{\partial\ \ln(F_R^{vp}F_\Theta^{vp}F_Z^{vp})}{\partial t} = 0 \quad (27)$$

After using the initial condition for the viscoplastic deformation gradient ($F_R^{vp} = F_\Theta^{vp} = F_Z^{vp} = 1$ at $t = 0$), the

TABLE I
Dimensionless Variables and Parameters Used

Dimensionless variables	Dimensionless parameters
Solvent concentration $c \equiv c_s/c_s^0$	Equilibrium concentration $c_{eq} \equiv c_g^\infty/(Hc_s^o)$
Time $\tau \equiv Dt/l_0^2$	Initial volume fraction $\beta_i \equiv \overline{V}_s c_s^o$
Location $\eta \equiv r/l(t)$	Mass Biot number $Bi_m \equiv k_g l_0 H/D$
Surface position $\lambda \equiv l(t)/l_0$	Initial polymer position $\eta_0 \equiv R/l_o$
Pressure $\hat{\pi} \equiv \pi/G$	Elasticity number $N_{El} \equiv Gl_o^2/(\mu D)$

product of these components is always a unity throughout the drying process:

$$F_R^{vp} F_\Theta^{vp} F_Z^{vp} = 1 \quad \text{at all} \quad t > 0 \tag{28}$$

This confirms the initial application of incompressible viscoplastic deformation as in eq. (7). Hence three unknowns (F_R^{vp}, F_Θ^{vp}, F_Z^{vp}) are governed by the combination of eq. (28) with any two of the three ordinary differential eqs. (24–26), the solution of which describes the development of the stress-free state. For centrally symmetric spheres, $F_Z^{vp} = F_\Theta^{vp}$, and eqs. (24–26 and 28) can be further simplified to an algebraic equation and an ordinary differential equation. Here they are kept general as above to consider both fibers and spheres. The coupling of these equations about the stress-free state and the diffusion equation system (1–4) are enough to describe the one-dimensional stress development in the drying axially symmetric fibers or centrally symmetric spheres.

Dimensionless simplification

For polymer–solvent systems, the diffusion coefficient, shear modulus, viscosity, and yield stress are all functions of solvent concentration. As a first approximation, constant material properties are used. The dimensionless variables and parameters used in the computation are listed in Table I.

The resulting dimensionless equation system is

$$\frac{\partial c}{\partial \tau} = \frac{1}{\lambda^2}\frac{1}{\eta^\omega}\frac{\partial}{\partial \eta}\left(\eta^\omega \frac{\partial c}{\partial \eta}\right) + \frac{\eta}{\lambda}\frac{d\lambda}{d\tau}\frac{\partial c}{\partial \eta} \tag{29}$$

$$\frac{d\lambda}{d\tau} = -\beta_i Bi_m (c - c_{eq}) \tag{30}$$

$$\alpha = \left(\frac{1-\beta_i}{1-\beta_i c}\right)^{1/3} \tag{31}$$

$$\frac{\partial \eta}{\partial \eta_o} = \alpha^3 \left(\frac{\eta_o}{\eta}\right)^\omega \tag{32}$$

$$\frac{1}{F_R^{vp}}\frac{\partial F_R^{vp}}{\partial \tau} = \frac{N_{El}\alpha^3}{6}\frac{\langle \Phi - k\rangle}{\Phi}(2B_R^e - B_\Theta^e - B_Z^e) \tag{33}$$

$$\frac{1}{F_\Theta^{vp}}\frac{\partial F_\Theta^{vp}}{\partial \tau} = \frac{N_{El}\alpha^3}{6}\frac{\langle \Phi - k\rangle}{\Phi}(-B_R^e + 2B_\Theta^e - B_Z^e) \tag{34}$$

$$F_Z^{vp} = \frac{1}{F_R^{vp} F_\Theta^{vp}} \tag{35}$$

$$\frac{\partial \hat{\pi}}{\partial \eta} = \frac{4B_R^e}{\alpha}\frac{\partial \alpha}{\partial \eta} + \frac{2\omega\alpha}{\eta (F_R^{vp})^2}\left(\frac{\eta_o}{\eta}\right)^{\omega-1} - \frac{(B_R^e + B_\Theta^e)\omega}{\eta} - \frac{2B_R^e}{F_R^{vp}}\frac{\partial F_R^{vp}}{\partial \eta} \tag{36}$$

The boundary and initial conditions are

$$c(\eta, 0) = 1, \quad \lambda(0) = 1 \tag{37}$$

$$c_\eta(0, \tau) = 0, \quad \frac{f}{1-\beta_i c} c_\eta(1, \tau) = -\lambda Bi_m (c - c_{eq}) \tag{38}$$

$$F_R^{vp} = F_\Theta^{vp} = F_Z^{vp} = 1 \quad \text{before yielding} \tag{39}$$

Among the above equations, the diffusion eqs. (29, 30) can be solved for solvent concentration independent

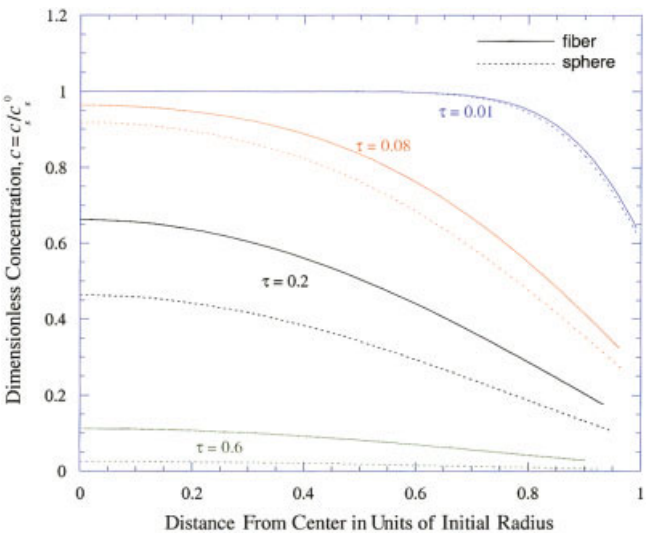

Figure 2 Concentration distribution along radius of fiber/sphere after different intervals of drying.

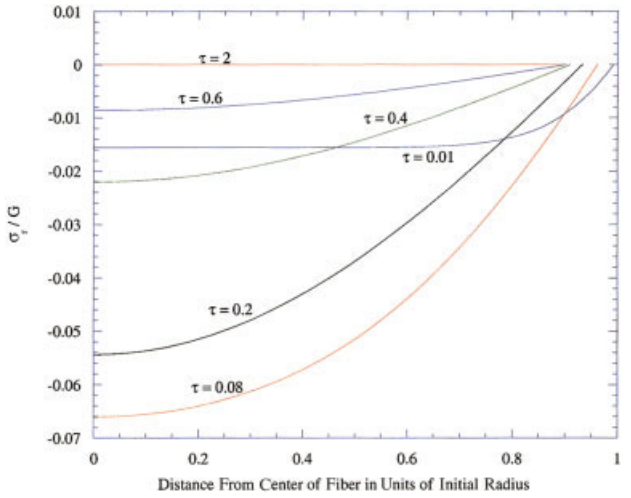

Figure 3 Radial stress distribution along radius of elastic fiber after different intervals of drying.

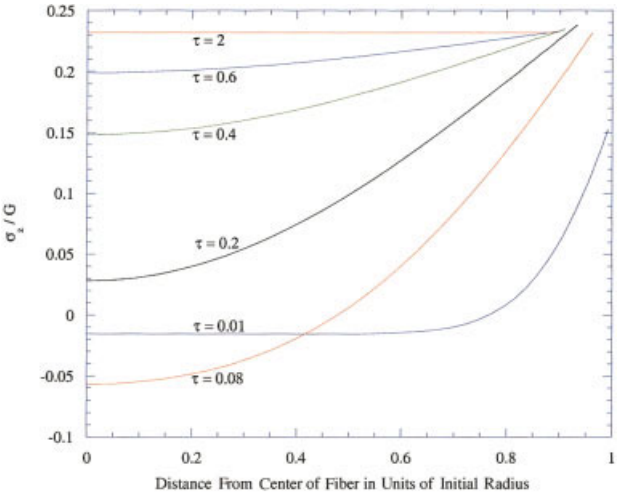

Figure 5 Axial stress distribution along the radius of elastic fiber after different intervals of drying. This stress keeps the fiber in plane–strain condition.

of the rest of the equation set, from which the concentration distribution and free surface position are given. Then the local volume shrinkage can be easily evaluated through eq. (31). The integration of eq. (32) then gives the current coating particle position (η) of the same particle originally located at η_o. Hence, the solvent concentration distribution, the local volume shrinkage, and the current coating particle position are available before solving for stress, largely simplifying the numerical calculations. The reason for this simplification is that the stress does not accelerate or hinder the diffusion, and elastic and viscoplastic deformations do not change the volume of the coating. Once the amount of local volume shrinkage and the current coating particle position are available, the two ordinary eqs. (33, 34) and the algebraic eq. (35) can be solved for the evolution of the stress-free state. Pressure then can be determined by solving eq. (36). Finally the stress distributions are computed from simple substitutions.

A finite element program similar to that used by Lei and coworkers[7,8] was developed to solve for the drying and stress development in axisymmetric fibers and centrally symmetric spheres.

RESULTS AND DISCUSSION

Elastic fibers/spheres

For an elastic fiber/sphere, a trivial solution will occur in the limiting case when diffusion resistance within the fiber/sphere is small compared to the mass transfer resistance in the air, so that the concentration of

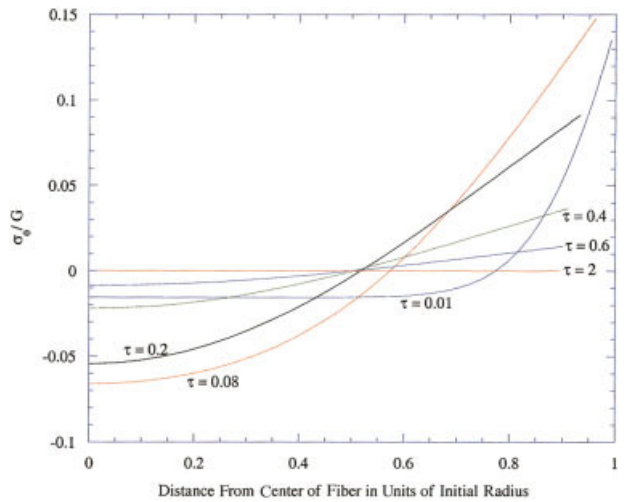

Figure 4 Tangential (hoop) stress distribution along elastic fiber after different intervals of drying.

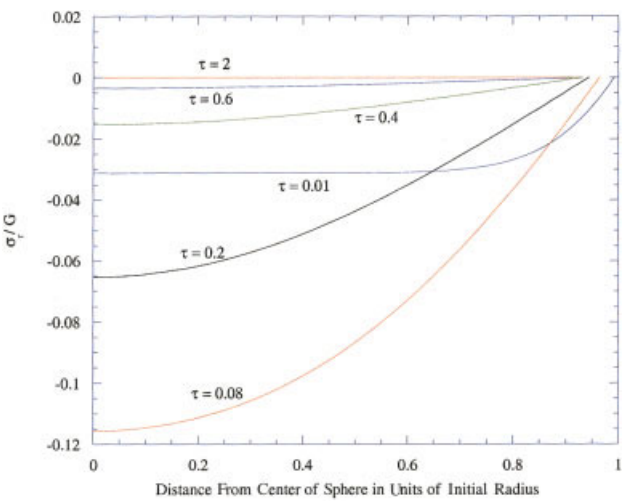

Figure 6 Radial stress distribution along radius of elastic sphere after different intervals of drying.

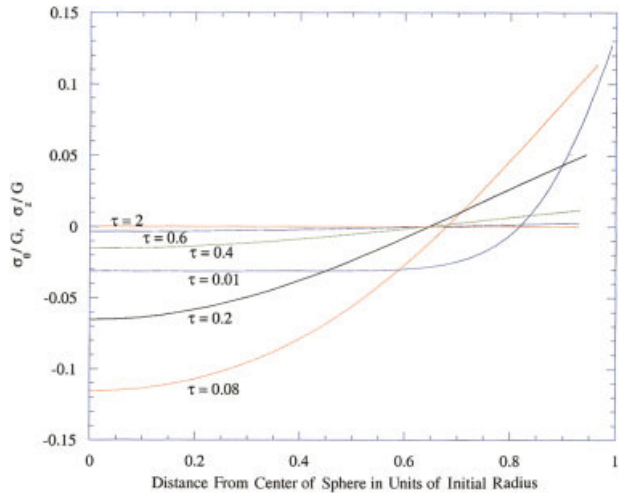

Figure 7 Tangential (hoop) stress distribution along radius of elastic sphere after different intervals of drying.

solvent can be considered as invariable with the position. In this limiting case, the shrinkage ratio does not vary with radius. Solving the above boundary value problem gives

$$\eta = \alpha^{3/(1+\omega)}\eta_o, \quad \hat{\pi} = \alpha^{(4-2\omega)/(1+\omega)} \tag{40}$$

Substituting these into eq. (13), one can find all stress components. For fibers ($\omega = 1$), the only non-zero component of the Cauchy stress tensor is

$$\sigma_z = -G\alpha + \frac{G}{\alpha^2} \tag{41}$$

This comes from the constraints at the two ends of the fiber, since the two ends have to be fixed in order to keep the fiber under plane–strain condition. For spheres ($\omega = 2$), all stress components are zero, which is reasonable since the sphere has neither shrinkage gradient nor frustration from any substrate.

When diffusion resistance within is comparable to the mass transfer resistance in the air, the concentration of solvent is no longer uniform. Figure 2 shows the concentration profiles in the fiber/sphere taken at four different dimensionless times, $\tau = 0.01$, $\tau = 0.08$, $\tau = 0.2$, $\tau = 0.6$. In the computation, the coating initially consists of 20 vol % solvent and 80 vol % polymer; the convective air is dried so that $c_{eq} = 0$. The mass Biot number is chosen as $Bi_m = 5$, so drying is diffusion-dominated. At the beginning stage of drying (e.g. $\tau = 0.01$), a large driving force causes rapid solvent depletion near the surface, resulting in a steep concentration gradient near the coating/air interface. In the late stages of drying (e.g. $\tau = 0.6$), almost all solvent is depleted and the concentration profile is flat throughout the coating. By comparing the concentration profile of a sphere to that of a fiber, it is found that drying a sphere is faster than drying a fiber with the same radius and drying conditions. This is reasonable because the sphere has a larger surface area per unit volume as compared with that of the fiber.

As drying continues and the solvent concentration gradient develops, the local volume shrinkage varies along the radius. For fibers, this non-uniform shrinkage is another source of stress, in addition to the frustration at both ends. For spheres, this non-uniform shrinkage is the only source of stress. Figures 3–7 show the stress distributions in the fiber and sphere at six different times. Initially, at the start of drying, the fiber/sphere is in the stress-free state, both radial and hoop stresses being zero. As drying starts, the solvent evaporates from the free surface and the material close to the free surface shrinks more than the material near the center of the fiber/sphere. As a result, the polymer particles near the center are squeezed by the outer particles, and simultaneously the outer particles are extended by the inner ones. This interaction gives a negative radial stress, σ_r (Figs. 3 and 6), that reaches a minimum at the center and trends to zero at the free surface to be consistent with the non-traction boundary condition there. The hoop stress (σ_θ) (Figs. 4 and 7), however, is positive near the surface and negative near the center, because the material near the surface is under tension and the material near the center is squeezed. The total hoop force, or the area integral of hoop stress along the radius, should vanish in order to maintain equilibrium in the fiber/sphere.

As drying continues, the radial stress becomes more negative and the hoop stress deviates further from the initial zero value. However, this process continues only to a certain point. When more and more solvent evaporates from the fiber/sphere and the amount of residual solvent diminishes, the solvent concentration and volume shrinkage become more uniform. Thereafter, the stress distribution approaches the solution of an elastic fiber/sphere under uniform shrinkage, in which for a fiber the only non-zero stress is the axial stress and for a sphere the stresses decrease back towards zero.

For drying fibers, the distribution of axial stress (σ_z) is shown in Figure 5. Stress results from the constraint of the two fixed ends. Immediately after the drying begins, the axial stress is positive near the free surface, which suggests that the coating particles near the free surface are under axial tension. In the center of the fiber, however, the particles are under axial compression. After a certain drying time, the whole fiber is under axial extension. The total forces that must be applied to the ends of the fiber are the area integral of axial stress over the end surfaces.

To more clearly present the changing of stresses during the drying process, the stress evolution profiles at three coating particles in the fiber/sphere are

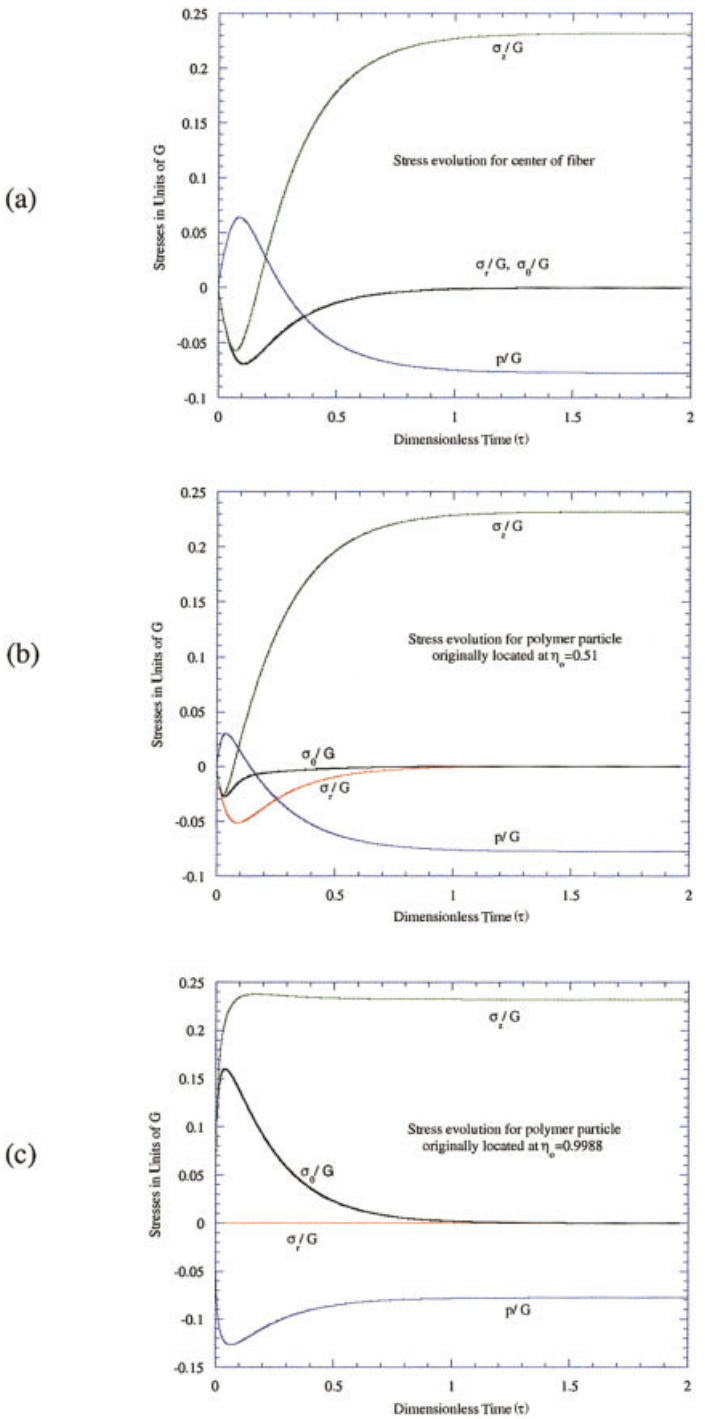

Figure 8 Stress evolution for coating particles of elastic fiber originally located at: (a) center of the fiber; (b) $\eta_o = 0.51$, near midpoint between center and free surface; and (c) $\eta_o = 0.9988$, near free surface of fiber.

plotted in Figures 8 and 9. The first particle is located at the center ($\eta_o = 0$) of the fiber/sphere [Figs. 8 and 9(a)], the second one is originally located near the mid point ($\eta_o = 0.51$) between the center and the free surface [Figs. 8 and 9(b)], and the third one ($\eta_o = 0.9988$) is originally located near the free surface [Figs. 8 and 9(c)]. From the development of stresses in fibers, the stresses are dominated by axial stress, which is developed to keep the fiber in a plane–strain condition. For the sphere, the center is under isotropic compressive stress, and the free surface is under aximuthal tension. They also show that the stresses change rapidly near the free surface. The stress evolution patterns are quite different at different positions. For example, close to the free surface, the hoop stress increases to a maximum,

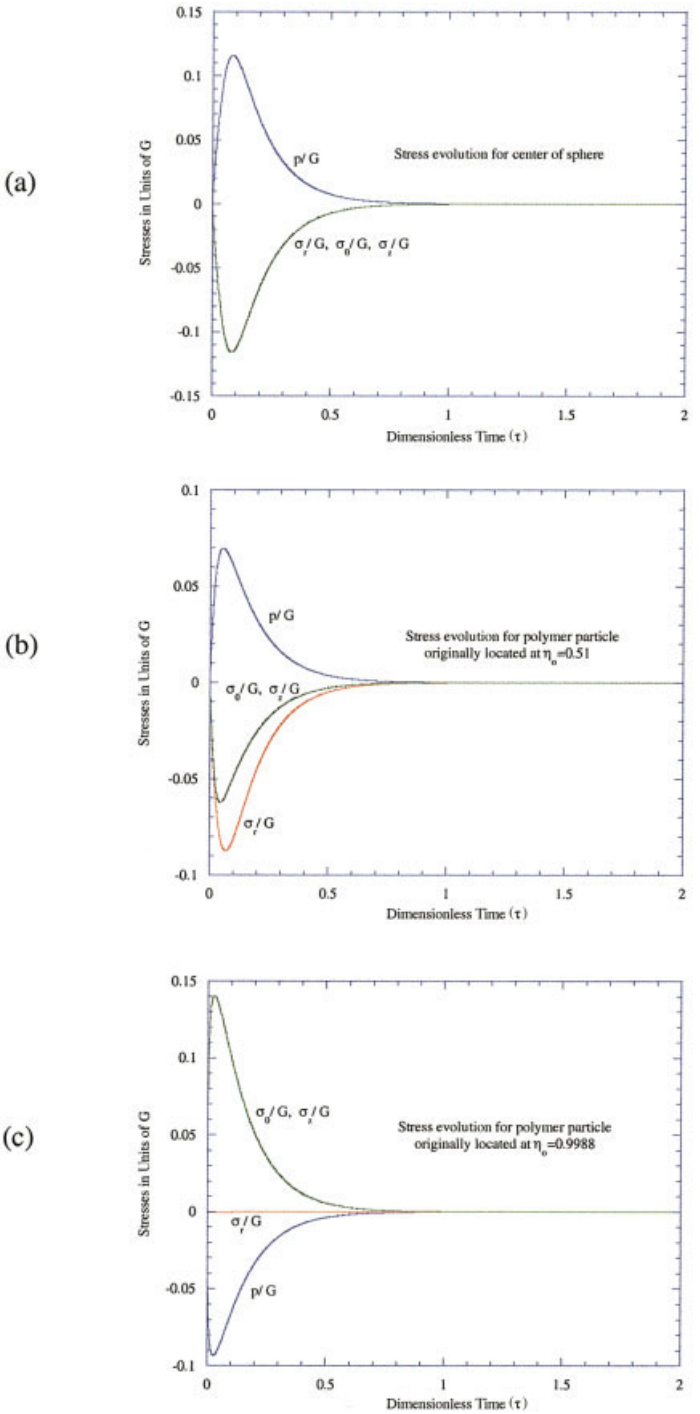

Figure 9 Stress evolution for the coating particles of elastic sphere originally located at: (a) the center of the sphere; (b) $\eta_o = 0.51$, near midpoint between center and free surface; and (c) $\eta_o = 0.9988$, near free surface of sphere.

then decreases to zero. Close to the center, however, it decreases to a minimum, and then increases to zero.

Elasto-viscoplastic fibers/spheres

Elasto-viscoplastic behavior appears when the second invariant of the local stress tensor in the fiber/sphere exceeds the local yield stress. Figures 10–14 show the stress distributions in a drying elasto-viscoplastic fiber/sphere at different times. Parameters used in the computation are $Bi_m = 5$, $c_{eq} = 0$, $\beta_i = 0.2$, $N_{El} = 4$, and $k = 0.02G$. A simple comparison in stresses between an elastic fiber/sphere (Figs. 3–7) and an elasto-viscoplastic fiber/sphere (Figs. 10–14) shows that the final stress distribution is uniform in an elastic fiber/

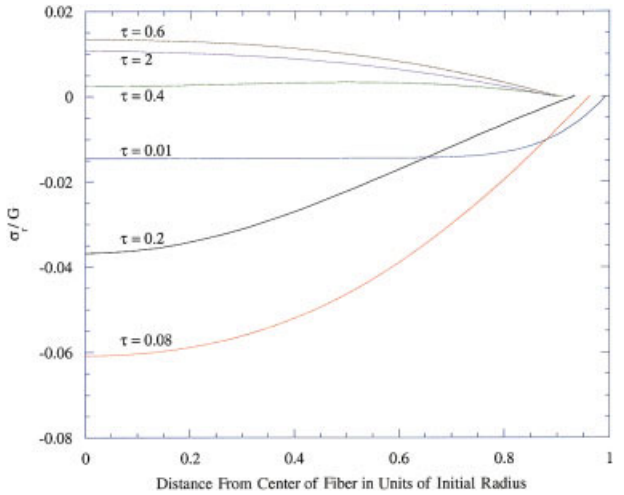

Figure 10 Radial stress distribution along radius of elasto-viscoplastic fiber after different intervals of drying.

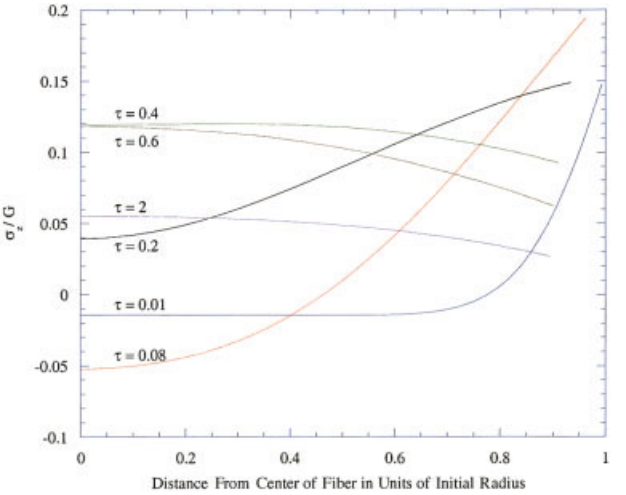

Figure 12 Axial stress distribution along radius of elasto-viscoplastic fiber after different intervals of drying. This stress keeps fiber in plane–strain condition.

sphere, but this is not the case in an elasto-viscoplastic fiber/sphere. For an elasto-viscoplastic fiber/sphere, the stress rises at the onset of drying due to the constraint from both ends of the fiber (no constraint for the sphere) and the non-uniform shrinkage as solvent evaporates. Once the stress exceeds the yield strength, the local material yields. The viscoplastic deformation, unlike the elastic deformation, is not reversible, and it dissipates some mechanical energy. The stresses vary with fiber/sphere radius, along with the amount of yielding and unrecoverable deformation. At a later stage of the drying, the shrinkage becomes more uniformly distributed due to the more uniform solvent concentration. As shown in Figures 10–14, the stress magnitude decreases and the material might go below the yield surface again, and the fiber/sphere is then subject to unloading. One major effect of stress unloading after yielding is the appearance of residual stress.

To more clearly explain this, we will focus on the development of hoop stress (Fig. 11 for a fiber and Fig. 14 for a sphere). At the very beginning of the drying, the polymer particles near the free surface are under hoop tensile stress due to the larger volume shrinkage close to the free surface as compared to that near the center of the fiber/sphere. At the same time, the polymer particles close to the center of the fiber/sphere are under compressive hoop stress. As more stress develops, the outer part of the coating yields, and then the yielding front propagates inward. After yielding, the decrease in hoop stress could be due to two factors. Firstly, when the drying is close to the end, the solvent concentration gradient and the volume shrinkage gra-

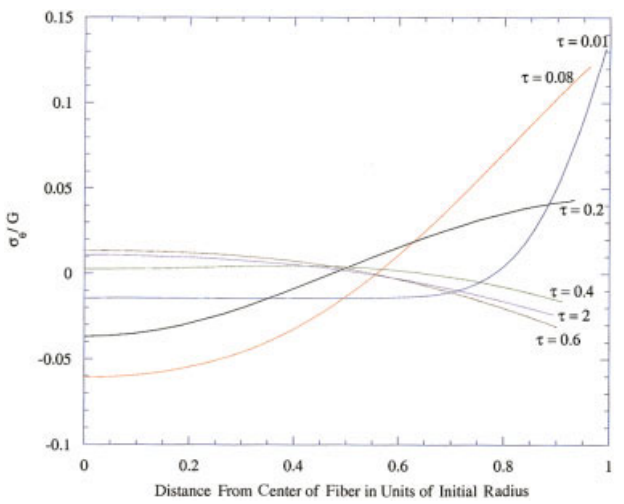

Figure 11 Tangential (hoop) stress distribution along elasto-viscoplastic fiber after different intervals of drying.

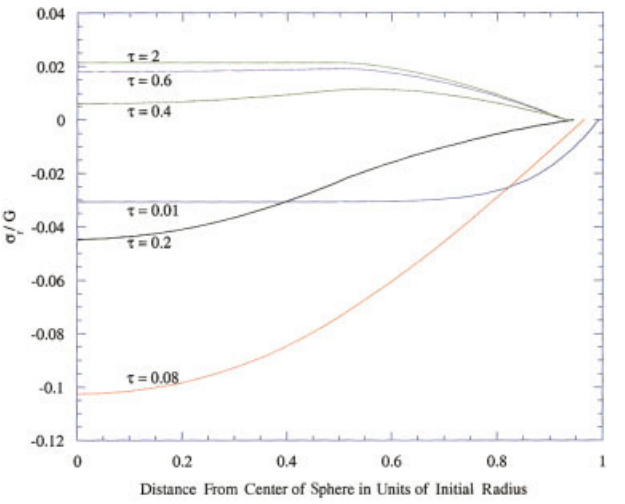

Figure 13 Radial stress distribution along radius of elasto-viscoplastic sphere after different intervals of drying.

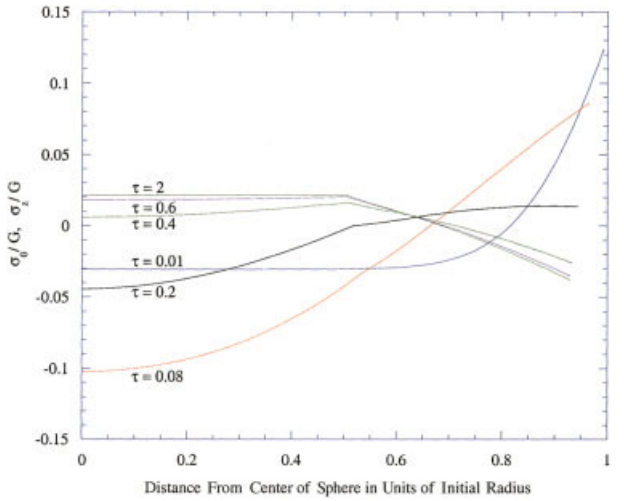

Figure 14 Tangential (hoop) stress distribution along radius of elasto-viscoplastic sphere after different intervals of drying.

dient become smaller, which give a lower stress. Secondly, when the second invariant of the stress tensor goes above the yield stress, the viscoplastic flow causes the stresses to relax. Since the viscoplastic deformation is not reversible, once the stresses at the yielded polymer particles become lower than the yield stress, unloading takes place. Different parts of the fiber/sphere may yield to different extents; therefore final residual stress will exist in the fiber/sphere. Note that the residual hoop stress near the free surface is compressive, while that near the center of the fiber/sphere is tensile. This is opposite to the hoop stress distribution at the beginning of the drying. This behavior of stress reversal is due to the interaction of the stresses among the circular/spherical layers in the drying fibers/spheres. This stress reversal behavior is not seen during the drying of a planar coating, since in it the equations governing the stresses are not interacting among the layers.[7]

CONCLUSIONS

Stress development in a drying fiber/sphere coating is due to non-uniform shrinkage as it dries and constraint from the surroundings. This study focuses on the drying after the coating solidifies, in which the coating is considered as an elasto-viscoplastic material. A large deformation elasto-viscoplastic model was developed to predict stress development in drying fibers and spheres.

Model predictions show that, during early stage of drying, hoop stresses in the fiber and sphere are tensile near the free surface and compressive near the center. Close to the end of drying, however, stress distributions will depend on coating materials. For elastic materials, stresses (except the axial stress that arises from the end constraints in elastic fiber coatings) decrease to zero due to the eventual uniform shrinkage. For elastoviscoplastic materials, residual stresses are presented even after the coating is completely dried. This is due to the varying levels of yielding at different locations. After drying of the elasto-viscoplastic materials, the model predicts a stress reversal behavior, where the particles near the surface are under compression and the particles near the center are under tension, reversed of what was observed during early stage of drying.

References

1. Charlesworth, D. H.; Marshall, Jr., W. R. Am Inst Chem Eng J 1960, 6(1), 9.
2. Crank, J. The Mathematics of Diffusion; Clarendon Press: Oxford, UK, 1975.
3. Okazaki, M.; Shoida, K.; Masada, K.; Toei, R. J Chem Eng Japan 1974, 7, 99.
4. Sano, Y.; Keey, R. B. Chem Eng Sci 1982, 37(6), 881.
5. Sano, Y. Drying Technology 1992, 10(3), 591.
6. Cairncross, R. A.; Francis, L. F.; Scriven, L. E. Drying Technology 1992, 10(4), 893.
7. Lei, H.; Payne, J. A.; McCormick, A. V.; Francis, L. F.; Gerberich, W. W.; Scriven, L. E. J Appl Polym Sci 2001, 81(4), 1000.
8. Lei, H.; Francis, L. F.; Gerberich, W. W.; Scriven, L. E. Am Inst Chem Eng J 2002, 48(3), 437.